High-Frequency Gap Losses in Nanocrystalline Cores

Yiren Wang, Gerardo Calderon-Lopez, and Andrew J. Forsyth, *Senior Member, IEEE*

***Abstract*—Finite element analysis is used to examine the gap losses that occur in finely laminated nanocrystalline inductor cores under high-frequency operation. The losses are seen to be concentrated in the region of the air gap and the dependence of the losses on key design parameters and operating conditions is explored. The results show that gap losses can be significant in this type of core, creating hot spots around the gap, and the losses are not accurately predicted by established design equations for low-frequency laminated cores. A modified loss equation is proposed. Validation is provided by measurements on a 300-A, 60 kHz inductor.**

***Index Terms*—DC inductor, finite element (FE) modeling, high-frequency gap losses, inductor design, nanocrystalline core.**

I. Introduction

NANOCRYSTALLINE cores such as Finemet from Hitachi Metals [1] and Vitroperm from Vacuumschmelze [2] are attractive for high-frequency high-power applications. They offer a high saturation flux density of over 1 T, and low hysteresis losses that are comparable with figures from some ferrites in the 20–100-kHz frequency range. Typical applications include inductors and transformers for multi-kilowatt DC–DC converters. These cores are wound from a thin (18 μm) metallic ribbon, each layer of the ribbon being insulated from the stack by a thin coating of epoxy. The cores therefore have a finely laminated structure and are typically available as C-cores.

While the hysteresis loss behavior of the cores has been thoroughly characterized [3]–[6] including the effects of nonsinusoidal excitation and dc bias, the phenomenon of gap losses is less well understood. These losses occur within the core near the air gap in the magnetic circuit and arise due to the fringing flux around the air gap. The fringe field creates a component of flux, B_n, which is normal to the surface of the ribbon laminations, Fig. 1, causing eddy currents and losses within the laminations. The effect can be particularly significant in some high-current, high-frequency dc inductors and increases with air gap length [7], [8]. Accurate prediction of these losses is, therefore, crucial for an optimum design. One approach to mitigate the effect is to place multiple smaller air gaps in the magnetic circuit; however, this may be difficult to manufacture and the multiple cuts can degrade the characteristics of the core [3], [4].

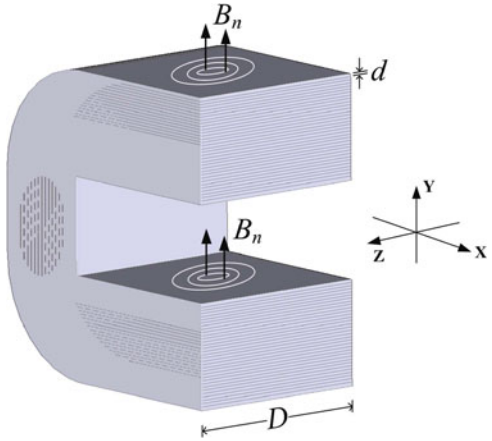

Fig. 1. Schematic diagram of in-plane eddy currents in one half of a cut core with air gaps.

This paper makes a contribution to the understanding and calculation of gap losses in nanocrystalline cores under high-frequency operating conditions. Finite element (FE) modeling is used to examine the distribution and magnitude of the gap loss in a Finemet C-core. A sensitivity study is undertaken using the simulation model to investigate the effects of the inductor design parameters, such as air gap length, frequency, flux density, and core lamination width, on the total gap loss. Assuming the gap loss is a power function of these parameters, a convenient design-oriented expression is derived for estimating gap loss at high frequency. Validation is provided by temperature measurements on a 300 A, 60-kHz inductor for a 30 kHz, 25-kW dual-interleaved DC–DC converter. The established gap loss calculation method is first reviewed, and then the inductor component is introduced followed by the details of the FE modeling.

II. Calculation of Gap Losses

The prediction of gap losses typically uses an empirical formula, (1), that was originally proposed by Lee in 1947 for steel laminated cores operating at power line frequencies [9]

$$P_g = G l_g D f {B_m}^2 \tag{1}$$

where P_g is the gap loss in Watts, l_g and D are the total gap length and lamination width in mm, respectively, B_m is the peak induction in the core in T with frequency f in kilohertz, and the term G is a numerical constant.

In the second edition of this book [10] (1955) Lee proposed a change to (1) whereby the frequency term was raised to the

Manuscript received April 14, 2016; revised June 13, 2016; accepted July 10, 2016. Date of publication August 30, 2016; date of current version February 11, 2017. This work was supported in part by the U.K. Engineering and Physical Sciences Research Council (EPSRC) Vehicle Electrical System Integration (VESI) project [EP/I038543/1] and also in part by the EPSRC National Centre for Power Electronics within the "Components Theme" [EP/K034804/1]. Recommended for publication by Associate Editor J. Acero.

The authors are with the School of Electrical and Electronic Engineering, The University of Manchester, Manchester M13 9PL, U.K. (e-mail: yiren.wang@manchester.ac.uk; gerardo.calderon-lopez@manchester.ac.uk; andrew.forsyth@manchester.ac.uk).

Color versions of one or more of the figures in this paper are available online at http://ieeexplore.ieee.org.

Digital Object Identifier 10.1109/TPEL.2016.2594083

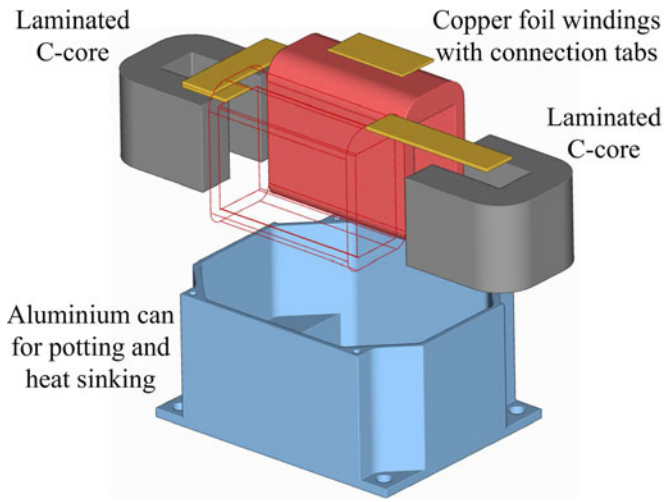

Fig. 2. Inductor structure.

power of 0.5 and also the lamination thickness and permeability were included; however, in subsequent publications in the 1970s [11], [12], he concluded that the original formulation was most accurate. This was based on testing both stamped lamination cores and strip wound cores of silicon steel at frequencies of 60 and 400 Hz. Lamination/Strip thicknesses of 360, 150, and 51 μm were used. Furthermore, different values were proposed for the constant G for various configurations of windings and air gaps, for example, $G = 0.388$ for single cut C-cores with two coils.

Equation (1) is generally used to predict gap losses in high-frequency inductor cores. The equation appears in McLyman's Transformer and Inductor Design Handbook [13], and it is used in the DC Reactor Core Design Tool from Metglas [14]. However, some concern has been expressed over the accuracy of (1) for high-frequency inductors using amorphous metal cores, suggesting the losses are likely to be much lower than predicted [4]. Other work has also suggested that the air gap fringing flux makes little contribution to the increased loss in cut nanocrystalline cores [3].

III. FE Gap Loss Modeling

A. Inductor Structure

The inductor component being analyzed consists of a pair of C-cores with series connected copper foil windings on each leg, Fig. 2. Each leg of the core has a gap of $l_g/2$, half the total gap length, and carries half of the winding. The winding is spaced away from the core by approximately the gap length per leg (l_g/2) to minimize the effect of the fringe field on the winding losses. The model was developed assuming a pair of F3CC-0032 Finemet cores [1], but is scalable to other core sizes. The total gap length l_g was initially set to 4.4 mm, with 2.2 mm in each leg. It was assumed that the complete component will be encapsulated in an aluminium can with thermally conducting epoxy, Fig. 2, however the can was not modeled.

B. Homogenization Modeling Method

Due to the fine laminations of the amorphous metal ribbon (18 μm thick), FE modeling the individual laminations was not considered feasible and instead a lumped parameter or homogenized approach was taken as illustrated in Fig. 3. The core was represented by a solid continuum, but the model preserves the anisotropic properties of the laminated structure through the use of separate permeability and electrical conductivity parameters in the directions tangential and normal to the lamination layers, μ_t, σ_t and μ_n, σ_n, respectively. The modeling approach is an established method for handling laminated cores and has been used in the analysis of the main eddy currents [15]–[17].

The amorphous metal ribbon itself has permeability and electrical conductivity μ_m and σ_m, while the insulating epoxy layers between the individual ribbons are assumed to have permeability μ_0, the permeability of free space, and an electrical conductivity of zero. Assuming that the packing factor F of the laminated core is defined as the total thickness of magnetic ribbon per unit of core thickness, then the parameters of the model may be calculated as in [15]

$$\mu_t = F\mu_m + (1-F)\,\mu_0 \tag{2}$$

$$\mu_n = \frac{\mu_m \mu_0}{F\mu_0 + (1-F)\,\mu_m} \tag{3}$$

$$\sigma_t = F\sigma_m \tag{4}$$

$$\sigma_n = \left(\frac{d}{D}\right)^2 \frac{1}{F}\sigma_m \tag{5}$$

where d and D are the thickness and width of the lamination strips, respectively.

The calculated parameters of the core model are listed in Table I assuming Finemet material characteristics of $\mu_m = 2500$, $\sigma_m = 8.33 \times 10^5$ S/m and a core packing factor of $F = 0.8$.

An effective skin depth, δ_e, for the laminated core may be calculated for the in-plane eddy currents using

$$\delta_e = \sqrt{\frac{2}{\omega \mu_n \mu_0 \sigma_t}} \tag{6}$$

where ω is the angular frequency of the core excitation. Based on the parameters in Table I, δ_e for Finemet material is 1.1 mm at 60 kHz.

C. Gap Loss Model

The whole inductor structure was modeled to establish the flux distribution in the magnetic circuit. The C-core structure was formed by several individual homogeneous blocks with ideal boundaries between each. Each block was modeled with homogenized anisotropic permeability and conductivity with a unique volume orientation to set up the direction of the laminations. To reduce the complexity of the problem, linear material properties were assumed. The copper foil winding was represented by current-driven Biot–Savart conductors carrying sinusoidal currents. The conductors were only used as magnetic sources in the model. The additional winding loss caused by the fringing flux was not investigated in this study. The regions surrounding the core and winding were simply modeled as free space. In practice these may be partly occupied by insulation or thermal potting materials.

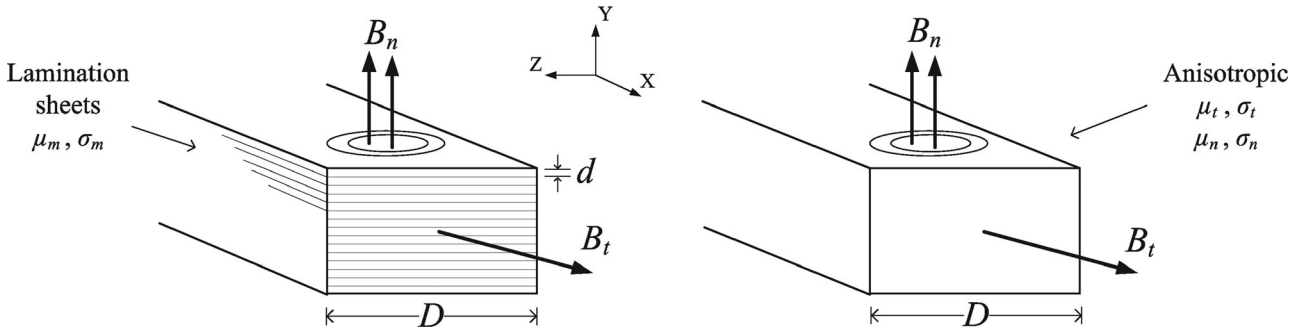

Fig. 3. Schematic diagrams of laminated core model. (Left) direct method. (Right) homogenization method.

TABLE I
EQUIVALENT MATERIAL PROPERTIES IN HOMOGENIZED FINEMET CORE MATERIAL ($\mu_m = 2500$, $\sigma_m = 8.33 \times 10^5$ S/M, AND $F = 0.8$)

Equivalent property	Value
μ_t	2000
μ_n	5
σ_t (S/m)	6.67×10^5
σ_n (S/m)	0.46

D. FE Mesh

The shape and size of the FE mesh was controlled to achieve good accuracy, while limiting the computational cost to a manageable level. In this model, the mesh size was set to 0.3 mm for the regions around the air gaps, which is about one-fourth of the equivalent skin depth at 60 kHz. A coarse mesh was used for the other regions which have smaller fringe field variations and were assumed to have minimal gap loss, and the maximum element size for the far end of the free air region was limited to 5 mm.

IV. GAP LOSS ANALYSIS

The 3-D gap loss model was solved in the Opera 3–D FEA software [18] using the steady-state electromagnetic solver, ELEKTRA/SS.

A. Perpendicular Flux Distribution

The overall magnetic field in the core is a combination of the source field created by the winding and that created by the induced eddy currents. To examine the source field that generates the eddy currents, the electrical conductivity of the core material was initially set to zero. As a result, the flux in the core was only induced by the source windings. The average flux density across the core cross-sectional area, B_m, was around 0.14 T.

Fig. 4 shows the perpendicular flux distributions through the middle of the core leg. The laminations are parallel with the *x*-axis. The perpendicular component is zero in the middle of the core leg and in the middle of the air gap, and it is largest at the core edges on the surfaces. The inner core surface, represented by the bottom edge in Fig. 4, has a slightly larger perpendicular flux distribution than the outer core surface (top edge) due to the proximity of the opposite core leg. The perpendicular flux component reduces as the measurement point moves away from the core gap edge into the air in the *y*-axis direction, and it reduces to about 10% of its peak value at $l_g/2$ away from the core, and to almost zero at a total gap length, l_g, away from the core.

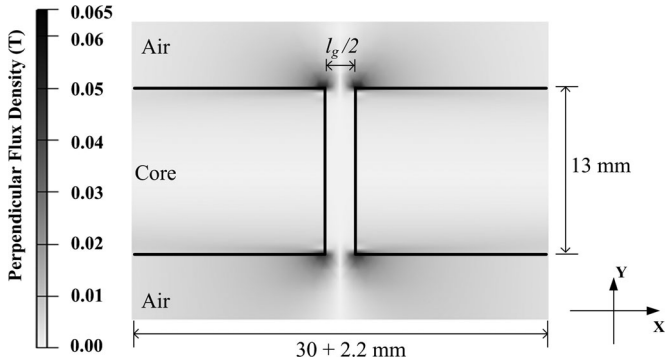

Fig. 4. Perpendicular flux distribution through the middle of the core leg, $l_g = 4.4$ mm, $B_m = 0.14$ T, and $f = 60$ kHz.

B. Eddy Current Distribution

To analyze the in-plane eddy currents, the anisotropic conductivities of the core material were restored. The eddy current distributions are consistent with the perpendicular flux distributions in Fig. 4 and are highly localized at the edges of the cores. To depict the eddy current distributions on the core surfaces, three surface views were created as shown in Fig. 5(a). The surface plots in Fig. 5(b) show the eddy current distributions looking down on the outer surface of the core (top plot), looking up on the inner surface (middle plot), and looking at the gap face (lower plot). The eddy current levels are slightly higher on the inner surface. The maximum current densities occur toward the center of the air gap edges and have values greater than 30 A/mm^2. The current densities are lower at the core corners, but increase along the side edges with maximum values in the region of 15 A/mm^2. The lower plot in Fig. 5(b) looking at the cut face of the core at the air gap shows that the eddy currents are concentrated within around 1.5 mm of the core edges.

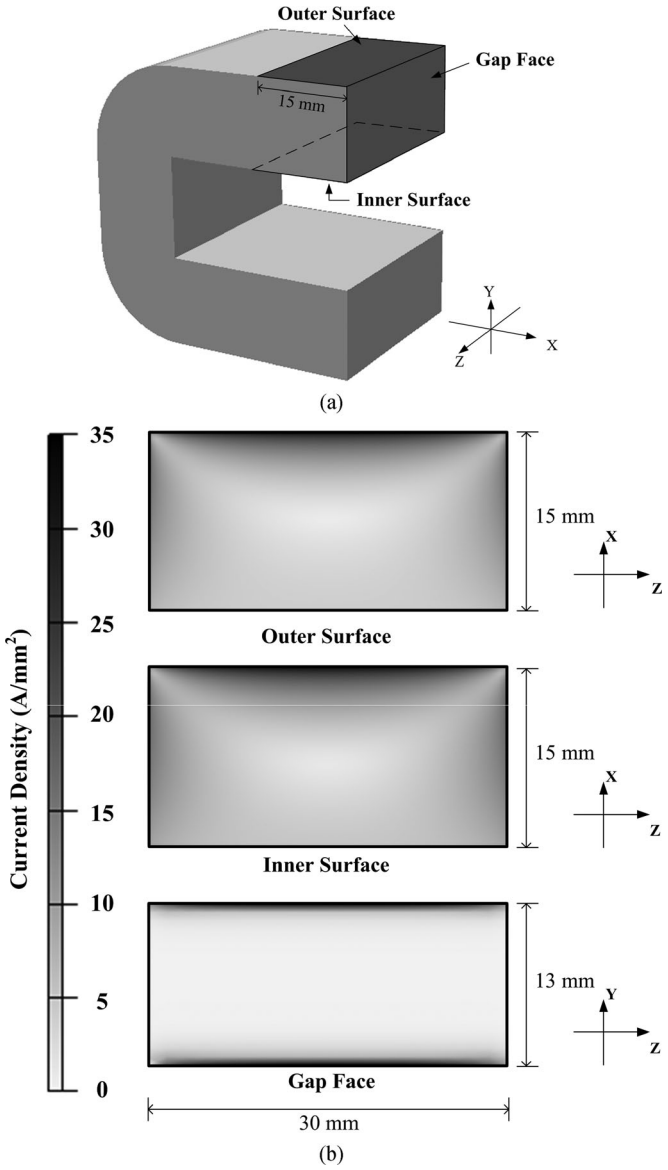

Fig. 5. (a) Outline of core surfaces. (b) Surface views of eddy current distributions, $l_g = 4.4$ mm, $B_m = 0.14$ T, $f = 60$ kHz.

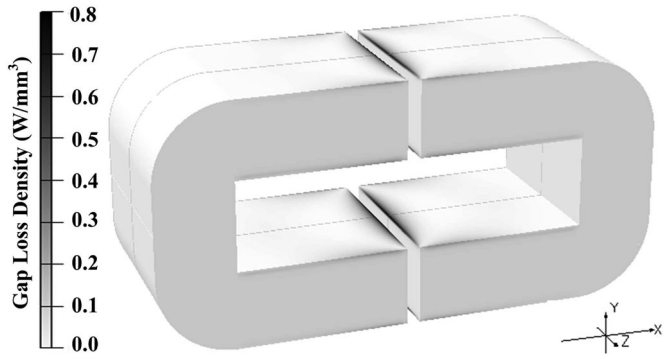

Fig. 6. Core view of gap loss distribution, $l_g = 4.4$ mm, $B_m = 0.14$ T, and $f = 60$ kHz.

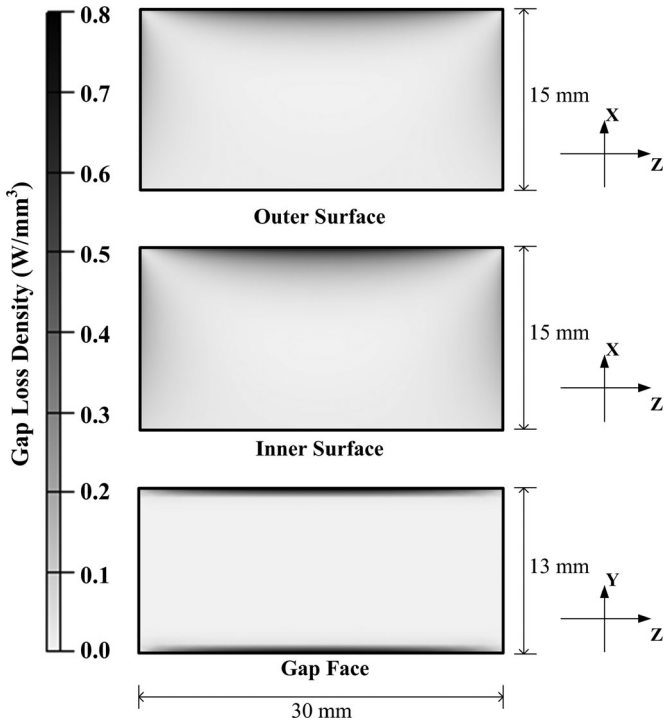

Fig. 7. Surface views of gap loss distribution, $l_g = 4.4$ mm, $B_m = 0.14$ T, $f = 60$ kHz.

C. Gap Loss Distribution

The loss density was calculated from time-averaged $\boldsymbol{J}\cdot\boldsymbol{E}$ in the simulations, where $\boldsymbol{J}$ and $\boldsymbol{E}$ are the vectors of current density and electric field strength, respectively. Fig. 6 shows the gap loss density in the core and the surface plots are shown in Fig. 7. The distribution of the gap loss corresponds to the eddy current density distributions. The maximum loss densities occur toward the center of the gap edges with a peak value of around 0.8 W/mm^3, and the side edges of the core also experience a high loss density of around 0.2 W/mm^3. The inner core surface (middle plot in Fig. 7) has a slightly broader loss distribution than the outer surface (top plot), and this is explained by the larger perpendicular flux distribution in the inner core surfaces. The bottom plot in Fig. 7 shows the loss distribution across the gap face, where the loss densities are concentrated within around 1 mm of the top and bottom gap edges. The total gap loss in the core was calculated by integrating the loss density over the core volume. At 60 kHz, the gap loss was calculated to be 44 W at a peak flux density of 0.14 T. The hysteresis loss at the same condition is 5 W based on a datasheet prediction. The gap loss, therefore, contributes a major part of the inductor core loss for the design example considered here. Furthermore, the hysteresis loss is distributed throughout the entire volume of the core while the gap loss is highly concentrated. Nearly 45% of the total loss is located around the core edges at the gap. About 15% of the loss is distributed along the core side edges. The rest of the loss is spread around the other parts of the core surfaces.

V. Gap Loss Prediction

The sensitivity of the gap loss to the inductor design parameters was investigated using FEA simulations. This was done

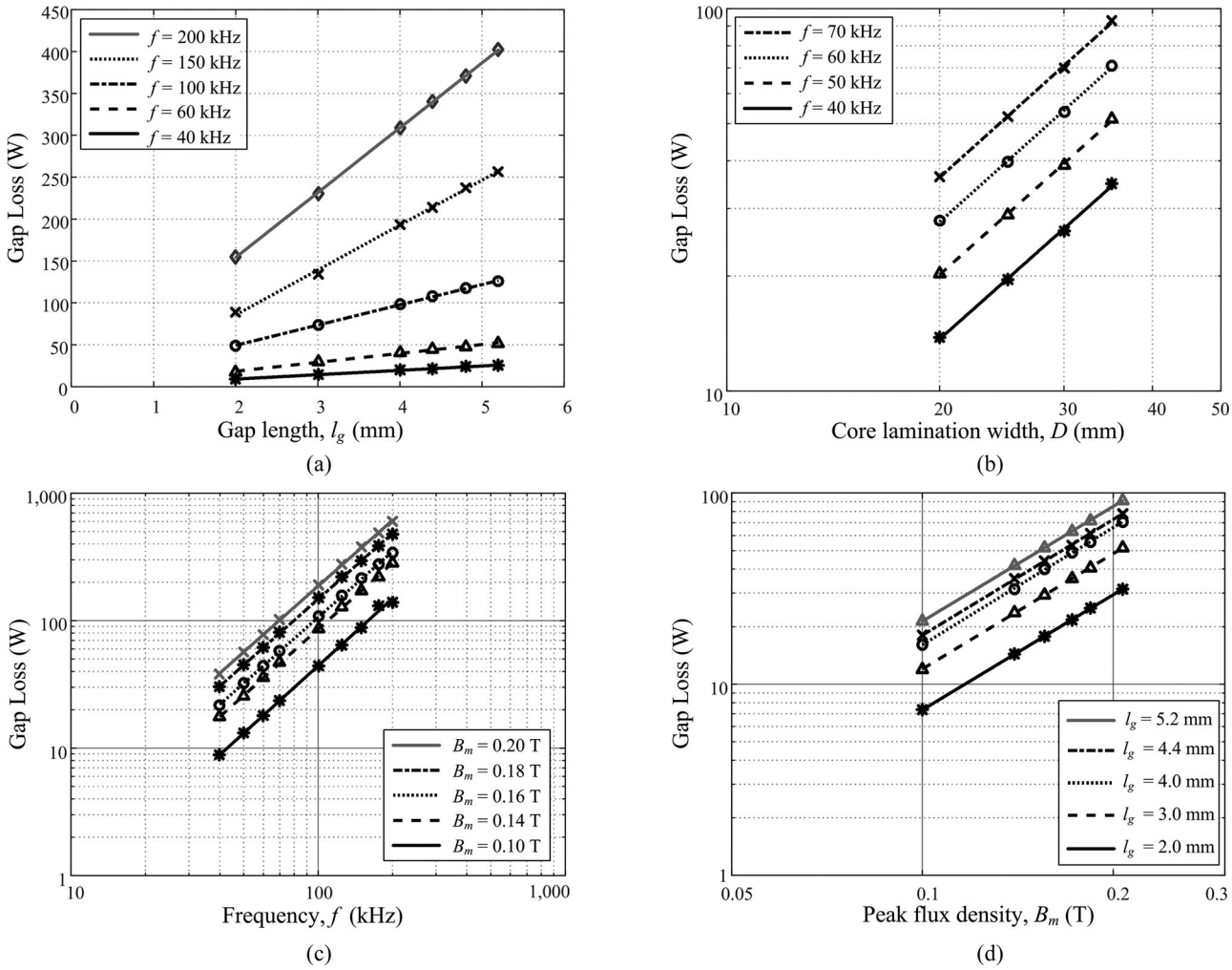

Fig. 8. Gap loss sensitivity analysis. (a) Gap loss variation with gap length, $D = 30$ mm, $B_m = 0.16$ T. (b) Gap loss variation with core lamination width, $l_g = 4.4$ mm, $B_m = 0.17$ T. (c) Gap loss variation with frequency, $l_g = 4.4$ mm, $D = 30$ mm. (d) Gap loss variation with peak flux density, $f = 60$ kHz, $D = 30$ mm.

by varying one inductor parameter while the others were kept constant. The preliminary assumption is that the gap loss can be expressed as a power function of the total gap length l_g, core lamination width D, frequency f, and peak ac induction B_m, as in (7), which is in line with the published equation, (1) [12]. In (7), k_g is a numerical constant, and k_{lg}, k_D, k_f, and k_{Bm} are assumed to be constants independent of each other representing the sensitivity of the gap loss to the inductor parameters. The values of these constants were determined by curve fitting the results from the sensitivity analysis

$$P_g = K\left(l_g,\ D, f,\ B_m\right) = \ k_g {l_g}^{k_{lg}}\ D^{k_D}\, f^{k_f}\, {B_m}^{k_{Bm}}. \quad (7)$$

Fig. 8 shows the variations of gap loss with the inductor design parameters. The gap loss is proportional to the gap length, as seen in Fig. 8(a). Varying the frequency changes the gradient of the lines but the proportionality is maintained. A similar pattern is seen with other parameters. Therefore, the exponent k_{lg} is equal to 1. For varying lamination width D from 20 to 35 mm, frequency f from 40 to 200 kHz, and the peak flux density B_m from 0.1 to 0.2 T, the fitted curves are straight lines with constant slopes in the log-log plots, Fig. 8(b)–(d). Varying other parameters moves the lines vertically but the slopes are unchanged. Therefore, the exponents k_D, k_f, and k_{Bm} are determined from the slopes of the fitted lines, and the gap loss is considered to be proportional to $D^{1.65}$, $f^{1.72}$, and B_m^2. The equation to estimate the gap loss can then be expressed as (8), where $k_g = 1.68 \times 10^{-3}$. Compared with the previous equation, (1) proposed by Lee, the derived loss expression shows the gap loss in high-frequency cores depending on the core width and frequency to the power 1.65 and 1.72, respectively, as opposed to linearly. Since the model assumes an ideal Biot–Savart current-driven winding, (8) excludes the effects of winding shielding and is, therefore, valid for inductors where the winding is spaced at least one gap length per leg away from the core

$$P_g = k_g l_g D^{1.65} f^{1.72} {B_m}^2. \quad (8)$$

VI. Experimental Validation

The FE gap loss model was validated on a purpose built inductor by temperature measurements. The predicted magnitude

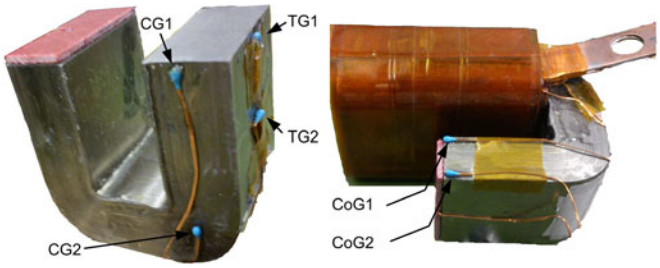

Fig. 9. Location of temperature sensors.

Fig. 10. Potted inductor on a heat sink with fan, thermal insulation not shown.

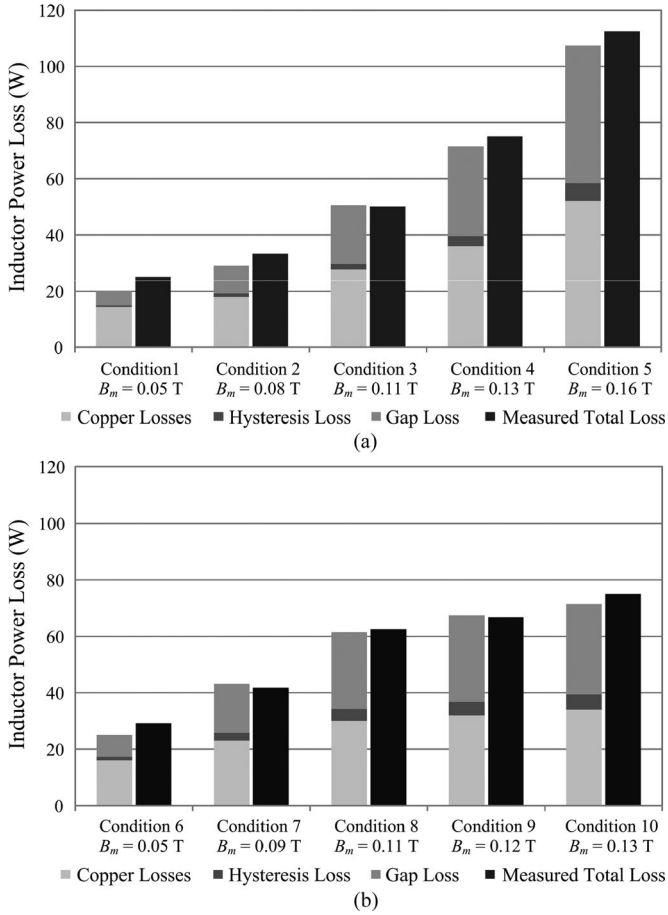

Fig. 11. Calculated and measured total inductor losses at 60 kHz. (a) 50% duty ratio conditions. (b) 20% duty ratio conditions.

of the gap loss was verified by comparing the measured and calculated total inductor losses, and the distribution of the gap loss was examined by measuring the steady-state core temperature at different locations on the core surface.

The inductor was designed for the input inductor for a 30 kHz, 25-kW dual interleaved DC–DC converter with interphase transformer [19]. The frequency in the inductor will be doubled to 60 kHz due to interleaving. Finemet F3CC-0032 cut cores were used and the two core halves were placed 2.2 mm apart to form a total gap length of 4.4 mm. The winding comprised six turns of 0.8-mm-thick and 51-mm-wide copper foil and was split between the two gapped core legs with three turns around each. The minimum space between the core and coils was 2.2 mm. The inductance was measured to be 5.1 μH at 60 kHz by a precision LCR meter.

Several temperature sensors were fixed to different locations on the core, especially around the gaps, to verify the temperature distribution, Fig. 9. NTC thermistors were used for the temperature measurements due to their superior immunity to ac magnetic field interference, attributed to their relatively large signal level. Furthermore, the data logger was operated with batteries to minimize common mode interference. The inductor was encapsulated in an aluminum can with thermally conductive epoxy resin potting material (1.8 W/mK). The potted component was mounted on a small aluminum heat sink cooled by a fan, Fig. 10, then covered with a thick layer of thermal insulation to ensure that all the heat was removed by conduction through the heat sink.

The component was operated on the DC–DC converter with an average input current of 160 A and varying ac excitation (by varying the converter input and output voltages) at two duty ratios, representing symmetric and asymmetric waveforms, respectively. Each test was run for at least 50 min at a continuous input power, ensuring that the inductor settled to steady state.

Fig. 11 compares the measured total inductor losses against the predictions at 60 kHz under two different duty ratio conditions. The measured power losses, shown as the black columns on the right, were determined from the measured steady-state temperature rises in the heat sink and the thermal resistance of the heat sink assembly, which was characterized thermally in a separate test with known power dissipation from dc power resistors. The calculated inductor losses include the hysteresis loss, copper loss, and gap loss, which are represented by the stacked columns in Fig. 11. The hysteresis loss was determined by separate measurements on an ungapped inductor wound on the same core using the B-H loop measurement method [5]. The copper losses were calculated from the published winding loss equations for foil wound inductors with nonsinusoidal waveforms [20], [21]. The dc winding loss was 12 W in all cases due

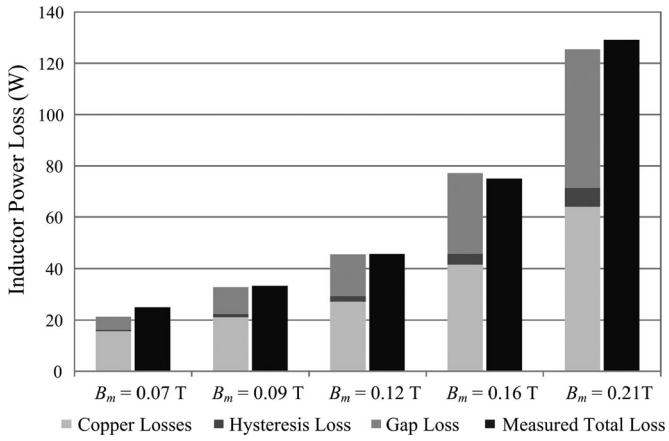

Fig. 12. Calculated and measured total inductor losses at 50 kHz, 50% duty ratio conditions.

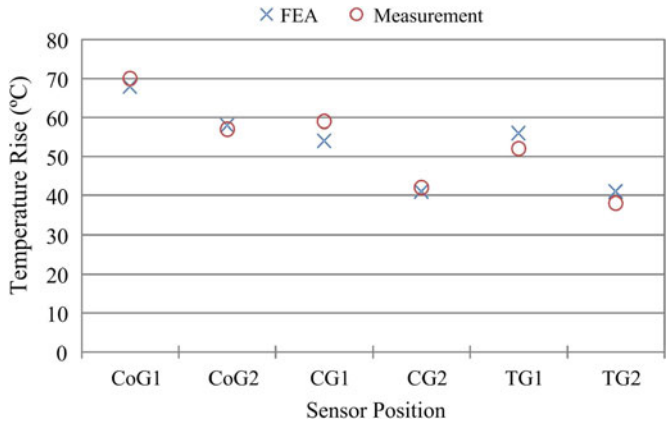

Fig. 13. Measured steady-state temperature rises on the core surface, heat sink temperature: 38 °C (Converter operating condition: $V_{\rm in}$ = 75 V, V_o = 275 V, switching frequency = 29.8 kHz, $I_{\rm dc}$ = 160 A, $I_{\rm pk-pk}$ = 130 A, B_m = 0.16 T).

to the constant dc current of 160 A. The ac winding loss including skin and proximity effects was calculated for the individual current harmonics using the one-dimensional Dowell analysis. The proximity effect accounted for approximately 98% of the ac winding loss. Air gap fringing losses in the winding were assumed to be negligible since there was a space of at least one gap length per leg between the core and winding. The gap loss was predicted using the FE model and (8). To account for the nonsinusoidal waveforms, the gap loss was approximated by the superposition of the losses calculated from the first three harmonic components of the actual waveform. Fig. 12 further validates the loss predictions at a different frequency, 50 kHz. Overall, the calculated total losses agree with the experimental measurements with an average error of less than 5%, and by implication the accuracy of the predicted gap loss is confirmed, particularly since the gap loss contributes a significant part of the total inductor loss in this example.

Fig. 13 compares the measured and predicted steady-state temperature rises above the heat sink at different sensor positions under the maximum ac flux condition at 160 A, 60 kHz. The loss information corresponds to Condition 5 in Fig. 11(a). The thermal prediction was carried out by a separate 3-D thermal FEA using the loss distribution results from the electromagnetic model. The measurements and predictions show excellent agreement.

The measured hot spot temperature is 108 °C at CoG1, which is a 70 °C temperature rise above the heat sink. The regions near the gaps, CoG1, CoG2, CG1, and TG1, experience the highest temperatures. By comparing CG1 and CG2, the core temperature reduces by 17 °C moving away from the gap along the middle of the core leg to the end of the core leg. On the outer core surface, the temperature drops by 14 °C from TG1 to TG2 moving halfway down the core leg from the gap. The high temperatures around the gap regions confirm the nonuniform gap loss distribution as predicted.

VII. Conclusion

A 3-D electromagnetic FE model has been developed to predict the gap loss distribution in finely laminated nanocrystalline inductor cores operating at high frequencies. The losses were seen to be highly localized on the edges of the core in the region of the air gap with loss densities approaching 1 W/mm^3 in the design example. Depending on the design parameters the gap loss can be a major part of the total inductor losses and accurate prediction is, therefore, important for optimized designs and to prevent localized overheating.

Based on the FE analysis, an updated approximation formula has been proposed for the estimation of gap losses in nanocrystalline cores. Since current-driven Biot–Savart conductors were used for the windings, the shielding effect of the winding on the gap fringe field is neglected. Therefore the results are applicable to inductors where the windings are spaced away from the core by approximately the gap length per leg. If the windings were closer to the core, the fringe field and gap loss would be reduced, but at the expense of increased winding loss. The FE model has been validated by measurements on a 5.1 μH, 300 A, dc inductor operating with 60 kHz ripple in a 30-kHz DC–DC converter. Since the FE model assumes single frequency sinusoidal excitation, the total gap loss was determined by adding the losses due to the first three harmonics using the approximation formula. The predicted overall losses matched closely with measurements, and furthermore the measured core temperature distribution corresponded closely with predictions from a 3-D FE thermal model.

The updated gap loss approximation formula is considered to provide a sound basis for the design and optimization of nanocrystalline core, high current dc inductors operating at frequencies up to around 100–200 kHz. The updated formula shows that the gap losses increase with strip width D to the power 1.65 as opposed to linearly in the established design equation. This suggests that a narrower strip width and a thicker core, having the same cross-sectional area may be beneficial in reducing gap losses.

References

[1] FINEMET® F3CC series cut core, Catalog., Hitachi Metals, Jan. 2010. [Online]. Available: www.hitachi-metals.co.jp

[2] Vacuumschmelze GmbH & Co. KG., 2011 [Online]. Available: www.vacuumschmelze.com
[3] S. Wei, W. Fei, D. Boroyevich, and C. W. Tipton, "Loss characterization and calculation of nanocrystalline cores for high-frequency magnetics applications," *IEEE Trans. Power Electron.*, vol. 23, no. 1, pp. 475–484, Jan. 2008.
[4] M. S. Rylko, B. J. Lyons, J. G. Hayes, and M. G. Egan, "Revised magnetics performance factors and experimental comparison of high-flux materials for high-current dc-dc inductors," *IEEE Trans. Power Electron.*, vol. 26, no. 8, pp. 2112–2126, Aug. 2011.
[5] J. Muhlethaler, J. Biela, J. W. Kolar, and A. Ecklebe, "Core losses under the dc bias condition based on steinmetz parameters," *IEEE Trans. Power Electron.*, vol. 27, no. 2, pp. 953–963, Feb. 2012.
[6] L. Jieli, T. Abdallah, and C. R. Sullivan, "Improved calculation of core loss with nonsinusoidal waveforms," in *Proc. Ind. Appl. Conf., 36th IAS Annu. Meeting*, 2001, vol. 4, pp. 2203–2210.
[7] H. Fukunaga, T. Eguchi, Y. Ohta, and H. Kakehashi, "Core loss in amorphous cut cores with air gaps," *IEEE Trans. Magn.*, vol. 25, no. 3, pp. 2694–2698, May 1989.
[8] H. Fukunaga, T. Eguchi, K. Koga, Y. Ohta, and H. Kakehashi, "High performance cut cores prepared from crystallized Fe-based amorphous ribbon," *IEEE Trans. Magn.*, vol. 26, no. 5, pp. 2008–2010, Sep. 1990.
[9] R. Lee, *Electronic Transformers & Circuits*, 1st ed. New York, NY, USA: Wiley, 1947.
[10] R. Lee, *Electronic Transformers & Circuits*, 2nd ed. New York, NY, USA: Wiley, 1955.
[11] R. Lee and D. S. Stephans, "Measurement of gap loss in current limiting transformers," in *Proc. Workshop Appl. Magn.*, 1972, pp. 77–81.
[12] R. Lee and D. Stephens, "Influence of core gap in design of current-limiting transformers," *IEEE Trans. Magn.*, vol. M-9, no. 3, pp. 408–410, Sep. 1973.
[13] W. T. McLyman, *Transformer and Inductor Design Handbook*, 3rd ed., New York: Marcel Dekker, 2004.
[14] DC Reactor Core Design Tool, ver. 3.1.0., 2009 [Online]. Available: http://hitachimetals.metglas.com
[15] W. Jian, L. Heyun, H. Yunkai, and H. Lei, "Numerical analysis of 3D eddy current fields in laminated media under various frequencies," *IEEE Trans. Magn.*, vol. 48, no. 2, pp. 267–270, Feb. 2012.
[16] H. Kaimori, A. Kameari, and K. Fujiwara, "FEM computation of magnetic field and iron loss in laminated iron core using homogenization method," *IEEE Trans. Magn.*, vol. 43, no. 4, pp. 1405–1408, Apr. 2007.
[17] K. Muramatsu, T. Okitsu, H. Fujitsu, and F. Shimanoe, "Method of nonlinear magnetic field analysis taking into account eddy current in laminated core," *IEEE Trans. Magn.*, vol. 40, no. 2, pp. 896–899, Mar. 2004.
[18] Opera Simulation Software. [Online]. Available: http://operafea.com
[19] G. Calderon-Lopez, A. J. Forsyth, D. L. Gordon, and J. R. McIntosh, "Evaluation of SiC BJTs for high-power DC–DC converters," *IEEE Trans. Power Electron.*, vol. 29, no. 5, pp. 2474–2481, May 2014.
[20] N. Kondrath and M. K. Kazimierczuk, "Inductor winding loss owing to skin and proximity effects including harmonics in non-isolated pulse-width modulated dc-dc converters operating in continuous conduction mode," *Power Electronics, IET*, vol. 3, no. 6, pp. 989–1000, 2010.
[21] M. S. Rylko, B. J. Lyons, K. J. Hartnett, J. G. Hayes, and M. G. Egan, "Magnetic material comparisons for high-current gapped and gapless foil wound inductors in high frequency dc-dc converters," in *Proc. IEEE Power Electron. Motion Control Conf.*, 2008, pp. 1249–1256.

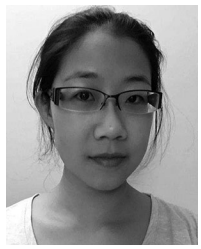

Yiren Wang received the B.Eng. (Hons.) degree from the University of Manchester, Manchester, U.K. and North China Electric Power University, Baoding, China, in 2011, and the Ph.D. degree from The University of Manchester, Manchester, U.K., in 2016.

She is currently a Research Associate at The University of Manchester. Her research interests include modeling, design and optimization of magnetic components for high power density DC–DC converters.

Gerardo Calderon-Lopez received the degree of Ingeniero en Comunicaciones y Electrónica from the National Polytechnic Institute, Mexico city, Mexico, in 1999, the M.Sc. degree in power electronics and drives from the Universities of Birmingham and Nottingham, U.K., in 2001, and the Ph.D. degree from The University of Manchester, Manchester, U.K., in 2009.

He is currently a Research Associate at The University of Manchester. His research interests include the design, modeling, simulation, control and optimization of hard and soft-switched DC/DC converters for electric vehicles, including their magnetic components.

Andrew J. Forsyth (M'98–SM'06) received the B.Sc.(Eng.) degree from Imperial College, London, U.K., in 1981 and the Ph.D. degree from the University of Cambridge, Cambridge, U.K., in 1987.

He was a Design Engineer with GEC Electrical Projects Ltd. from 1981 to 1983, a Lecturer at the University of Bath from 1986 to 1990, and a Lecturer/Senior Lecturer at Birmingham University from 1991 to 2004. Since 2004, he has been a Professor of power electronics at the University of Manchester, Manchester, U.K. His research interests include high-frequency converters and magnetic components, high-power-factor rectifiers, modeling and control of autonomous power systems, aerospace and electric vehicle applications.